Monte Carlo Track Structure Code for Low-Energy Alpha-Particles in Water

Shuzo Uehara[†] and Hooshang Nikjoo*[,‡]

School of Health Sciences, Kyushu University, Maidashi 3-1-1, Higashi-ku, Fukuoka 812-8582, Japan, and Medical Research Council, Radiation and Genome Stability Unit, Harwell, Oxfordshire, OX11 0RD, U.K.

Received: October 31, 2001; In Final Form: March 20, 2002

The paper describes the development of a new generation of Monte Carlo track structure code, which simulates full slowing down of low-energy alpha-particles history tracks (*leahist*) in the range 1 keV−8 MeV in water. All primary interactions including elastic scattering, ionization, excitation, and charge exchange by He^{2+}, He^{+}, and He^{0} were taken into account. Cross sections for bare and dressed helium ions and neutral helium impact were obtained from experimental data for water vapor targets. Where data were lacking the existing experimental data were fitted and extrapolated. The tracks of secondary electrons were generated using the electron track code *kurbuc*. The code can be operated to generate tracks both in the *track segment* and the *full-slowing-down* modes. Tracks were analyzed to provide confirmation on the reliability of the code and information on physical quantities, such as range, *W*-values, restricted stopping power and radial dose profiles. This new development enables us to work on aspects of the radiation of environmental interests such as radon. No attempt was made to simulate the track of alpha-particles below 1keV as in this region cross sections for interactions involving electron loss and capture are severely lacking and in general the chemistry which follows the interaction of these slow ions is not well-known.

1. Introduction

Over the past 3 decades many Monte Carlo track structure codes have been written to simulate the passage of charged particles in environments of interest to chemical, biological, medical, and other applications of practical interest. As knowledge of the physics and chemistry of interaction of charged particle in matter and speed of computers have increased, so has the range of applications of these codes. These computer simulation codes have mainly been used to study the nature of chemical and biological damage induced by ionising radiation and have contributed significantly to the understanding of the mechanism of radiation effects.[1−6]

To date, there are a number of Monte Carlo track structure codes for electrons[7−12] and ions[13−19] which have been developed independently to investigate the microscopic features of ionising radiation. All these codes provide coordinates of interactions, amounts of energy deposited and type of interaction at each event. Although inelastic collision cross sections used in electron codes are fairly similar for energetic electrons, there exists some differences among the codes at energies below 100 eV.[5] Our present knowledge of the physics, chemistry, and computational methods of electron track simulation is sufficiently advanced to provide the primary physical input to deal with the initial distribution of radical and molecular species in solution and induced initial yield, distribution and spectrum of damage in DNA by high and low LET radiations.[20] A common feature of all Monte Carlo track structure codes for ions (protons, alpha-particles, and heavy ions) is that they all simulate track segments and the effective energy range is limited to energies greater than 0.3 $MeVu^{-1}$. This is due to lack of cross sections for many of the important interactions at lower energies.[18]

Recent developments in Monte Carlo track structure simulation include calculation of theoretical cross sections, for the first time, for water below 0.3 $MeVu^{-1}$ by Uehara et al.[21] and Dingfelder et al.[22] The authors have evaluated cross sections for low-energy protons and neutral hydrogen, compiling experimental cross sections for water vapor because experimental data for liquid water are not available.[21,22] These reports produce theoretical stopping cross sections in good agreement with published data. On the bases of the evaluated cross sections, we have developed for the first time a new generation of Monte Carlo track structure codes for simulation of tracks of low-energy protons (the code *lephist*, *l*ow-*e*nergy *p*roton *his*tory *t*racks)[23] and alpha-particles (the code *leahist*, *l*ow-*e*nergy *a*lpha-particles *his*tory *t*racks, the subject of the present paper) in water. All major interactions including elastic scattering, excitation, ionization and charge exchange by the charged ion and the neutral atom were taken into account.

This paper describes a new model for the development and simulation of a full slowing down tracks of alpha-particles in the energy range 1 keV−8 MeV in water. The reliability of cross sections and energy transfers are examined by analytical calculations of the macroscopic stopping cross sections. Tracks of secondary electrons ejected by helium ions were simulated using the electron code *kurbuc*.[10] Various results such as range and *W*-values derived by analysis of simulated alpha tracks are presented and discussed.

2. Interactions of Low-Energy Alpha-Particles

2.1. Alpha-Particle Interactions. As charged particles pass through matter, they lose energy primarily through collisions with bound electrons. Ionization cross sections for the projectile and secondary electron energies are needed to follow the history of an incident particle and its products, covering all ranges of energy transfers in individual collisions. For fast alpha-particles, the majority of energy is transferred in ionising collisions,

* Corresponding author. Medical Research Council, Radiation and Genome Stability Unit, Harwell, Oxfordshire OX11 0RD, U.K. Tel: 44 1235 834 393. Fax: 44 1235 834 776. E-mail: h.nikjoo@har.mrc.ac.uk.
† School of Health Sciences.
‡ Medical Research Council.

10.1021/jp014004h CCC: $22.00
Published on Web 10/01/2002

TABLE 1: Interactions for Low-Energy He^{2+}, He^{+}, and He^{0} with Water

interactions	$He^{2+} + H_2O \rightarrow$	$He^{+} + H_2O \rightarrow$	$He^{0} + H_2O \rightarrow$
(i) elastic scattering	$He^{2+} + H_2O$	$He^{+} + H_2O$	$He^{0} + H_2O$
(ii) target ionization	$He^{2+} + H_2O^{+} + e$	$He^{+} + H_2O^{+} + e$	$He^{0} + H_2O^{+} + e$
target excitation	$He^{2+} + H_2O^{*}$	$He^{+} + H_2O^{*}$	$He^{0} + H_2O^{*}$
(iii) two-electron capture	$He^{0} + H_2O^{2+}$ (σ_{20})		
one-electron capture	$He^{+} + H_2O^{+}$ (σ_{21})	$He^{0} + H_2O^{+}$ (σ_{10})	
one-electron loss		$He^{2+} + e + H_2O$ (σ_{12})	$He^{+} + e + H_2O$ (σ_{01})
two-electron loss			$He^{2+} + e + e + H_2O$ (σ_{02})
(iv) one-electron capture and target ionization		$He^{+} + H_2O^{2+} + e$	$He^{0} + H_2O^{2+} + e$
one-electron loss and target ionization		$He^{2+} + e + H_2O^{+} + e$	$He^{+} + e + H_2O^{+} + e$

resulting in energetic free electrons and the potential energy of residual ions. Ionising collisions involving bare ion projectiles, unless they are very slow, can be treated by a classical description of the trajectory of the projectile with a quantal description of the target. ICRU[24] provides an excellent review of the availability and the features of electron spectra originating from ion collisions with atoms and molecules.

As fast ions slow, interactions involving electron capture and loss by the moving ions become an increasingly important component of the energy loss process. Charge transfer can produce residual ions without the release of free electrons, and free electrons can be ejected from the moving ion (or neutral) with no residual ions being formed. Charge transfer cross sections are generally designated as σ_{if} where i is the initial and f the final charge state of the moving particle. To develop track structure models, cross sections are needed for both electron capture and electron loss. For a complete description of the full slowing down of alpha-particles we need cross sections for one-electron capture (σ_{21}) and two-electron capture (σ_{20}) for He^{2+}, one-electron capture (σ_{10}) and one-electron loss (σ_{12}) for He^{+}, and one-electron loss (σ_{01}) and two-electron loss (σ_{02}) for He^{0}.

For incident alpha-particles with speeds comparable to or lower than the orbital speeds of bound electrons in the target, the capture of electrons from the target is a significant mechanism for the ionization of the target without production of secondary electrons. If the projectile is a dressed ion (i.e., an ion bearing one or more electrons), a collision can eject electrons from either the projectile or the target. For a fast projectile, one can consider the projectile as a simple collection of a nucleus and electrons travelling together at the same speed. After the charge transfer the dressed ion (He^{+}) or the neutral helium atom (He^{0}) becomes either stripped or ionizes a water molecule. In the former case, stripped ion, He^{2+} or He^{+}, an electron is ejected in a forward direction with nearly the same velocity as the projectile. In the latter case, ionization of water molecule without changing the ionic charge state, an electron is ejected with a different distribution of electron energy and with a similar ejection angle as that of the alpha-particle. Toburen[25] has published a comprehensive review of the basic data of interactions for low-energy ions in various media focusing on ionization and charge transfer. Similar to simultaneous target ionization, there could be a possibility of simultaneous target excitation for electron loss but not much information is available on this process.

In addition to information on ionization and other energy-loss processes, excitation cross sections for both helium ions and neutral helium were taken into account in this work. There are no reported experiments in the literature for excitation cross sections for alpha-particles impact on water. Therefore, we assumed that the total excitation cross sections for all helium projectiles are the same as those for protons. The proton cross sections were calculated using the model of Miller and Green[26] and a scaling procedure. More detailed description is given in section 3.3. Generally, high-energy ions proceed along a straight-line trajectory. However, the effect of elastic nuclear collisions (energy losses below 10 $keVu^{-1}$) cannot be neglected in the low-energy region. These elastic collisions might have a significant effect on the spatial character of the track structure at very low energies. In this work we assumed the direction of alpha-particle was not affected by inelastic events (ionization, excitation, and charge transfer at high as well as low-energy regions) but dominated only by the scattering angles in the laboratory system calculated by the theory of nuclear elastic scattering. By inelastic events we mean atomic collisions between the projectile and the orbital electrons of atom, not the nuclear inelastic events. In the early stages of the development of the theory and the code, we examined the simulated tracks of alpha-particles by taking into account not only the nuclear elastic collisions but also ion−molecule inelastic events. Angular deflections of alpha-particles were calculated using the kinematical relationship. The calculations showed unrealistic tortuous alpha tracks. Therefore, we adopted the assumption that the direction of alpha-particles are not affected by inelastic events.

Table 1 lists the primary interactions of low-energy helium ions with the stopping medium (water). The interactions include (i) nuclear elastic scattering; (ii) target ionization and excitation; and (iii) charge transfer for one-electron capture, two-electron capture, one-electron loss, and two-electron loss. Some data are available over most of the energy range of interest, and where data were lacking the existing data were fitted by a suitable function and extrapolated. Charge transfer can also be accompanied by simultaneous target ionization for both electron loss and electron capture processes (interaction iv, Table 1). However, there is insufficient information on cross sections for these interactions to be included in the calculations.

2.2. Electron Interactions. The transport of all secondary electrons is explicitly followed down to 1 eV using the Monte Carlo electron code *kurbuc*.[10] The code *kurbuc* simulates electron tracks in water vapor in the range 10 eV−10 MeV. The existing Monte Carlo electron track structure codes use a variety of theoretical models and assumptions in treating physical and chemical processes. Previously, we have examined the accuracy and predictive power of some of the existing Monte Carlo track structure codes.[27] The comparison and assessment of various experimental and theoretical approaches adopted in a number of Monte Carlo track structure codes were performed using the code *kurbuc* as an engine to observe the effect of the change of a set of cross sections on the output.[27] It was concluded that most codes produce tracks in good agreement with macroscopic quantities such as total stopping power (∼10%) and similar yield of strand breaks for both single and double strand breaks to within a few percentage of uncertainty.

3. Alpha-Particle Cross Sections

3.1. Charge Exchanges. *3.1.1. Total Cross Sections.* As low-energy charged particles pass through matter, they undergo

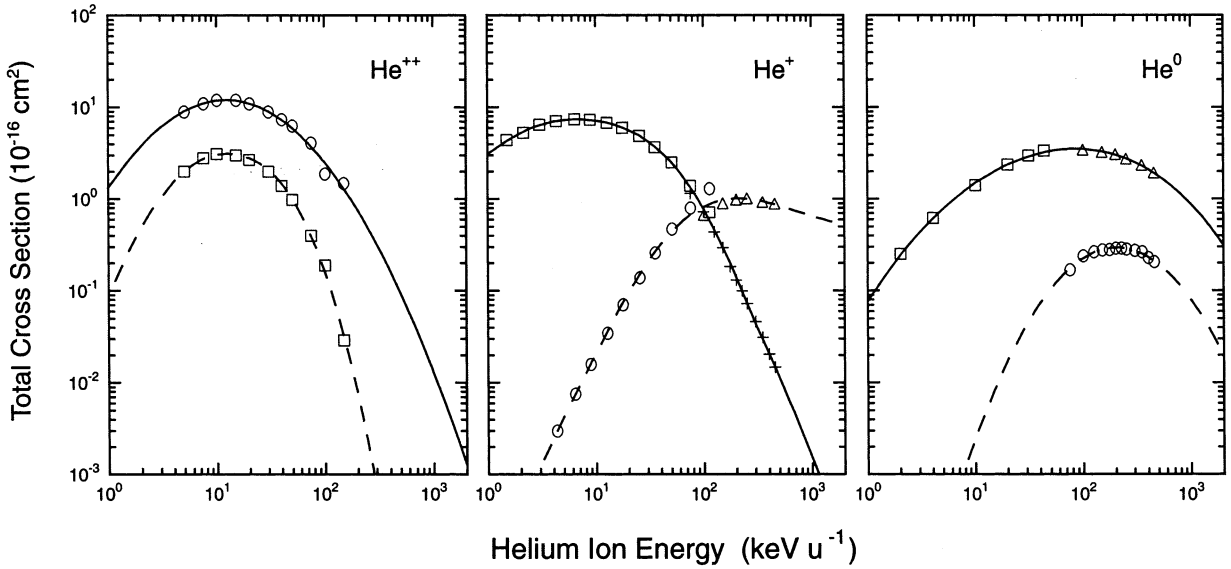

Figure 1. Charge exchange cross sections due to He^{2+} (left part), He^{+} (center part), and He^{0} (right part) impact on water vapor. The curves were fitted to experimental data by polynomial functions and extrapolated where data are lacking. Left part: − − − σ_{20} (this work), □ σ_{20} (expt) (ref 28), — σ_{21} (this work), ○ σ_{21} (expt) (ref 28). Center part: — σ_{10} (this work), □ σ_{10} (expt) (ref 30), + σ_{10} (expt) (ref 31), − − − σ_{12} (this work), ○ σ_{12} (expt) (ref 30), △ σ_{12} (expt) (ref 31). Right part: — σ_{01} (this work), □ σ_{01} (expt) (ref 32), △ σ_{01} (expt) (ref 31), − − − σ_{02} (this work), ○ σ_{02} (expt) (ref 31).

electron capture and loss events. Figure 1 shows six charge exchange cross sections based on available experimental data for He^{2+} (left part), He^{+} (center part) and He^{0} (right part). Experimental cross sections for one-electron capture (σ_{21}) and two-electron capture (σ_{20}) for He^{2+} are given by Rudd et al.[28] in the energy range 5 to 150 $keVu^{-1}$ in water. These cross sections were least-squares fitted by simple polynomial functions of the form $\log \sigma_{if} = \Sigma c_j (\log T)^{j-1}$, where log is to the base 10, and T in $keVu^{-1}$. We omit individual numerals for parameter c_j for all cases in this paper. At energies below 5 $keVu^{-1}$ and above 150 $keVu^{-1}$, these functions were extrapolated assuming a smooth transition at the boundaries. Cross sections for one-electron capture (σ_{10}) and one-electron loss (σ_{12}) for He^{+} were fitted to the experimental data of Rudd et al.[30] measured between 1 and 100 $keVu^{-1}$ and Sataka et al.[31] between 75 and 500 $keVu^{-1}$. In the latter, H_2O data were obtained by the additivity rule from the relationship $\sigma(H_2) + \sigma(O_2)/2$ using the measured values for H_2 and O_2. Extrapolation was made for the energies greater than 500 $keVu^{-1}$. Electron loss cross section (σ_{01}) for He^{0} was least-squares fitted using experimental data of Allison[32] below 100 $keVu^{-1}$ and Sataka et al.[31] between 75 and 500 $keVu^{-1}$. In the former, H_2O data was obtained from the relationship $2\sigma(H) + \sigma(O)$ using the measured values for H and O. Cross sections for two-electron loss (σ_{02}) were fitted to the data of Sataka et al.[31] Smooth extrapolation was carried out where the experimental data were lacking. Figure 2 shows calculated and experimental[29] equilibrium charge fractions as a function of helium ion energy. Calculations were carried out using eqs 21−22.

3.1.2. Energy Transfer Model. The energy deposition ΔE in electron capture was assumed to be equal to the average binding energy of a water molecule.

$$\Delta E = \bar{B}_{H_2O} \tag{1}$$

where $\bar{B}_{H_2O}$ is the weighted mean of the binding energies $\Sigma p_i B_i$, in which p_i is the fractional ionization cross sections for four outershells. The binding energy B_i was calculated using the Rudd model (eqs 3 and 4).[33] For alpha-particles, eq 1 is applied to the interactions σ_{21} and σ_{10}. We assume the energy deposition

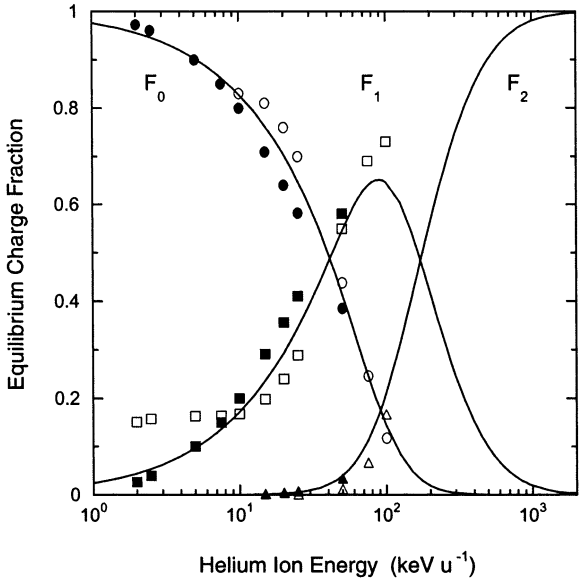

Figure 2. Equilibrium charge fractions of helium beam in H_2O calculated by eqs 21 and 22 in comparison with the experimental data in H_2 and O_2.[29] — this work, experimental data in H_2 (○ He^{0}, □ He^{+}, and △ He^{++}), in O_2 (● He^{0}, ■ He^{+}, ▲ He^{2+}).

for two-electron capture (σ_{20}) becomes $2\bar{B}_{H_2O}$ because H_2O^{2+} ion is generated. In the electron loss for neutral hydrogen, an electron is generated with the energy

$$\epsilon = T/\lambda \tag{2}$$

in which T is kinetic energy of the projectile in eVu^{-1}, and $\lambda = m_H/m_e = 1836$ where m_H and m_e are the masses of hydrogen atom and electron, respectively. For helium ions, eq 2 holds if units of eVu^{-1} is used for T. However, λ should be replaced by $\lambda' = m_{He}/m_e = \lambda(m_{He}/m_H) = 3.971\lambda$ and T (eV). The energy of the electron generated in the σ_{12} and σ_{01} interactions is T/λ'. While two electrons are emitted with the same energy and the same direction in the two-electron loss process (σ_{02}), in fact the stripped electron is observed in the spectrum of secondary electrons produced in $H^{\circ} + H_2O$[34,35] and in $He^{+} + H_2O$[36] interactions as a peak centered at T/λ'.

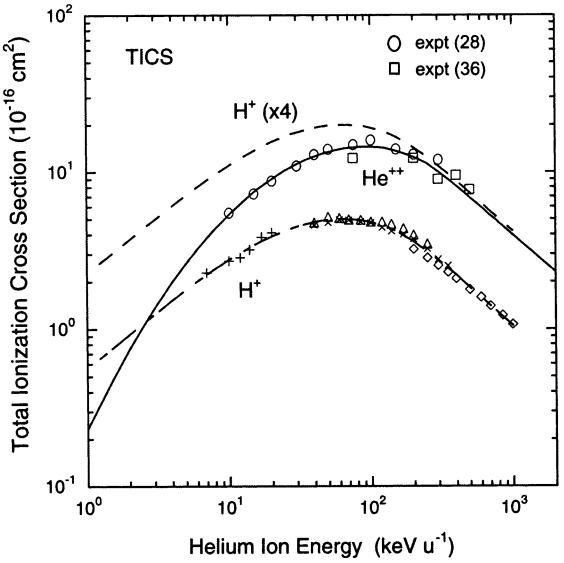

Figure 3. Total ionization cross sections due to He^{2+} impact on water vapor. The curve for the He^{2+} was obtained by fitting a polynomial function to the experimental data (refs 28 and 36) and extrapolated where data are lacking. The fitted cross sections were compared with the H^+ data multiplied by 4 according to Z^2 scaling as suggested by Rutherford theory. H^+ data were obtained from Uehara et al.[21,23] Data shows the evidence for Z^2 scaling at the high energy (>500 keV) region.

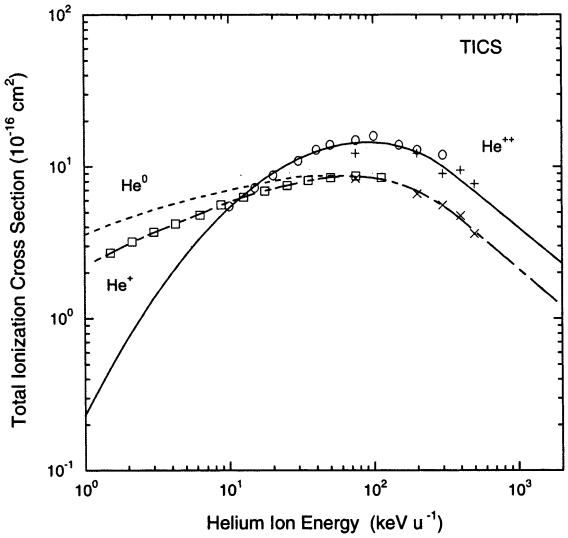

Figure 4. Total ionization cross sections due to He^{2+}, He^+, and He^0 impact on water vapor. Experimental data were taken from refs 28, 30, and 36. Cross sections for He^0 were adjusted to reproduce stopping cross sections for the lower energy alpha-particles and assumed to be the same as the He^+ cross sections for energies >100 $keVu^{-1}$. — He ++ (this work), ○ He^{2+} (expt) (ref 28), + He^{2+} (expt) (ref 36), — — — He^+ (this work), □ He^+ (expt) (ref 30), × He^+ expt (ref 36), — — — He^o (this work),

The emission direction of the stripped electron is assumed to be the same as the projectile. All data regarding this electron, the kinetic energy T/λ', the direction and the position are documented in the output file together with the secondary electrons due to ionization by helium ions and the neutral helium.

3.2. Ionization. *3.2.1. Total Cross Sections.* To obtain total ionization cross sections (TICS) for He^{2+}, we fitted a polynomial function to the experimental data of Rudd et al.[28] (measured between 10 and 300 $keVu^{-1}$) and data of Toburen et al.[36] (measured between 75 and 500 $keVu^{-1}$). At energies below 10 $keVu^{-1}$ smooth extrapolation was made. For energies greater than 500 $keVu^{-1}$, extrapolation was made by taking into account both the reproducibility of stopping powers and the scaling of proton ionization cross sections. Figure 3 shows a comparison of TICSs of water vapor by He^{2+} and H^+ (x4), in which H^+ data was determined by least-squares fitting to the experimental data given by Rudd et al.[37] The H^+ data are multiplied by 4 to scale according to Z^2 as suggested by the Rutherford theory.[24] It was found that the scaling law holds asymptotically at energies higher than 1 $MeVu^{-1}$. The rapid decrease shown in the lower energies reflects the competition between electron capture and direct target ionization. In this competition electron capture is largely the dominant partner.

Total ionization cross sections for He^+ were fitted to the experimental data of Rudd et al.[30] measured between 1 and 100 $keVu^{-1}$ and Toburen et al.[36] between 75 and 500 $keVu^{-1}$. The reason for this is that experimental cross sections for He^0 ionization are not available. Therefore, TICSs for He^0 at energies lower than 100 $keVu^{-1}$ were adjusted to fit the electronic stopping powers tabulated in ICRU Report 49.[38] In the region below 30 $keVu^{-1}$ the stopping cross sections: for He^{2+} are negligible; for He^+ ions are reliable and for He^0 are the main contributor. This point has been elucidated further in the discussion section. At energies above 100 $keVu^{-1}$, the total cross sections were assumed to be the same as those of He^+. Figure 4 shows calculated TICSs for this work and comparison with three sets of experimental data. The relative magnitude of the He^0 cross sections adopted here seems to be in good agreement with the experimental TICSs for He ions.[39,40]

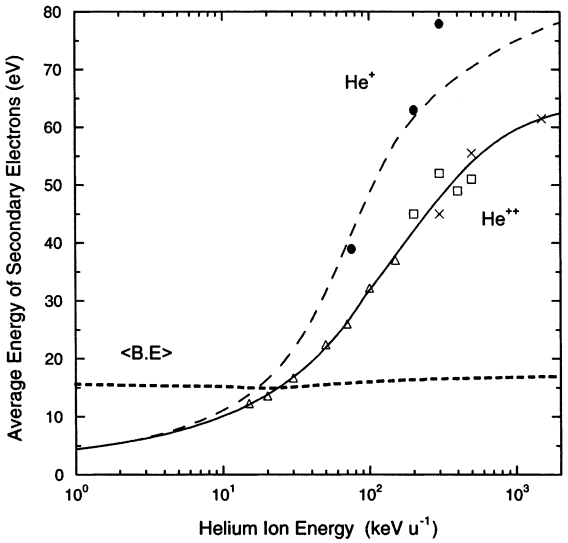

Figure 5. Average energy of secondary electrons ejected by helium ion impact on water vapor. (—, this work) Least-squares fitting for He^{2+} was carried out including the experimental data of (□) Toburen et al.[36] and for (△) H^+ of Bolorizadeh and Rudd[41] and (×) Toburen and Wilson.[42] Average energies for He^+ were calculated using the modified Rudd model (eqs 5 and 6), (— — —) calculations, (●) experimental data of Toburen et al.[36] (- - -) The average binding energy (16 eV) was calculated using model of Rudd for water molecule.

3.2.2. Average Energy and Energy Spectra for Secondary Electrons. Figure 5 shows the experimental data of average energy of secondary electrons ejected by alpha-particle impact[36] together with the experimental average energies by proton impact.[41,42] The average energies ejected by He^{2+} impact (□) at several hundred $keVu^{-1}$ of ion energies are almost the same as those by proton impact (×, △) within experimental uncertainties. Including the proton data, experimental average energies of secondary electrons due to He^{2+} impact were least-squares fitted (solid line), while the curve for the He^+ (dashed line)

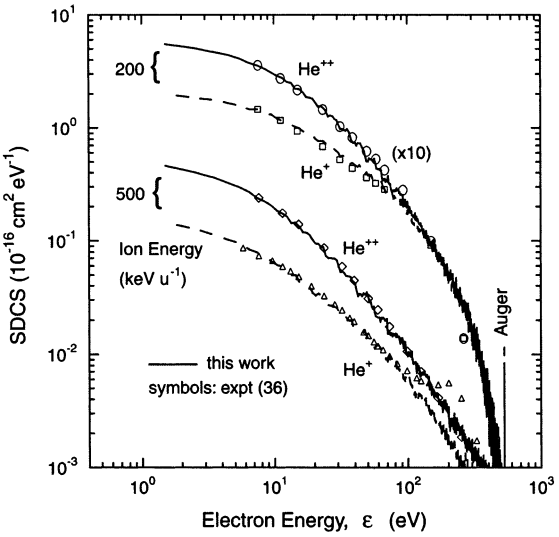

Figure 6. Randomly sampled energy spectra for secondary electrons ejected by helium ion impact with energies 200 and 500 keVu^{-1} in comparison with the experimental data of Toburen et al.[36] The lines are the results obtained from sampling 5×10^5 times using eqs 3−6.

was derived from the calculations using eq 6. The average energy of secondary electrons is required in the calculations of stopping cross sections (see section 3.5).

The similarity of average energies for ejected electrons suggested that the spectral difference between proton impact and alpha-particle impact is insignificant. Toburen et al. showed the ratio of single differential cross sections for electron emission (SDCS) for equal velocity protons and He^{2+} ions are distributed in the range 1.0 ± 0.2 for various projectile energies.[36] As a first approximation, Rudd's model[33] of proton impact was applied to the SDCS for He^{2+} impact ionization given by

$$\frac{d\sigma_i(\epsilon)}{d\epsilon} = \frac{S}{B} \frac{F_1 + F_2 w}{(1+w)^3\{1+\exp[\alpha(w-w_c)/v]\}} \qquad (3)$$

where ϵ = electron energy; B = binding energy for each orbital; $a_0 = 0.529 \times 10^{-8}$ cm; N = electron number in orbital; R = 13.6 eV; and $w = \epsilon/B$, $v = (T/\lambda B)^{1/2}$, $w_c = 4v^2 - 2v - R/4B$, $S = 4\pi a_0^2 N(R/B)^2$,

$$F_1(v) = L_1 + H_1$$
$$L_1 = C_1 v^{D_1}/(1 + E_1 v^{D_1+4})$$
$$H_1 = A_1 \ln(1+v^2)/(v^2 + B_1/v^2) \qquad (4)$$
$$F_2(v) = L_2 H_2/(L_2 + H_2)$$
$$L_2 = C_2 v^{D_2}$$
$$H_2 = A_2/v^2 + B_2/v^4$$

The fitting parameters for water vapor are given by Rudd et al.[43]

$$A_1 = 0.97 \quad B_1 = 82 \quad C_1 = 0.40 \quad D_1 = -0.30 \quad E_1 = 0.38$$
$$A_2 = 1.04 \quad B_2 = 17.3 \quad C_2 = 0.76 \quad D_2 = 0.04 \quad \alpha = 0.64$$

For ion energies lower than 300 keVu^{-1}, the model of Rudd reproduces well the average energies of secondary electrons. As energy of He^{2+} increases, at energies greater than 300 keVu^{-1}, the model underestimates the average energies up to ~30% at 2 MeVu^{-1}. To correct this discrepancy, calculated electron spectra were modified to produce the average energies using suitable scaling factors (for each ϵ for a certain impact energy). This procedure is equivalent to a parallel shift of energy spectrum to the right-hand side by about 10−30% for energies 500−2000 keVu^{-1} in the plot of SDCS vs ϵ (Figure 6).

Toburen et al. have provided the ratios of SDCSs for ionization of water vapor by He^+ to those for He^{2+} as a function of the ejected electron energy.[36] For ejection of low-energy electrons, i.e., small energy loss by the ion, the ratio decreases due to the screening of the nuclear charge by the He^+ bound electron. This ratio is distributed linearly from 0.4 to 1 for $0 < \epsilon < 90$ eV for various projectile energies between 200 and 500 keVu^{-1}. For ejection of fast electrons, the cross-sectional ratio approaches 1. Thus, the energy spectra for secondary electrons due to He^+ impact were obtained by modifying the Rudd's model (eqs 3 and 4) using a simple function $g(\epsilon)$ such that

$$\frac{d\sigma_i^{He^+}(\epsilon)}{d\epsilon} = g(\epsilon)\frac{d\sigma_i(\epsilon)}{d\epsilon} \qquad (5)$$

in which

$$g(\epsilon) = 0.4 + \epsilon/150 \quad \text{for} \quad \epsilon < 90 \text{ eV}$$
$$= 1 \quad \text{for} \quad \epsilon \geq 90 \text{ eV} \qquad (6)$$

The mean energies derived from the spectra agree well with the experimental data at 75 and 200 keVu^{-1}.[36] The average energies at higher He^+ energies were adjusted to fit the stopping cross sections. The experimental average energy of secondary electrons, 78 eV, at 300 keVu^{-1}, shown in Figure 5, is higher than the calculated data because this value includes contributions from the stripped electrons with energy $T/\lambda = 163$ eV.

The boundary energy for energetic secondary electrons generated by ionization was determined to be 1 eV. If electron energy is below 1 eV, then the energy deposition is $\Delta E = B_i + \epsilon$ for the ith orbital ionization. The secondary electron energy was sampled by a storage and look-up method in the Monte Carlo track code. Figure 6 presents the randomly sampled energy spectra of ejected electrons by He^{2+} (solid lines) and He^+ (dashed lines) at $T = 200$ and 500 keVu^{-1} in comparison with the experimental data of Toburen et al.[36] The experimental data includes contributions from all five orbitals of water molecule. Similarly, calculations of SDCS takes into account the relative intensity of partial ionization cross sections. Data obtained from 5×10^5 times sampling were normalized for the overall fitting to the experimental values. A good agreement shows the appropriateness of the present spectra (Figure 6). In these calculations we assumed the spectra of electrons ejected from the target molecule by He^0 impact to be equal to that for He^+.

3.2.3. Angular Distributions for Secondary Electrons. ICRU[24] has recommended a semiempirical formula (Hansen-Kocbach-Stolterfoht or HKS model)[44] for the double differential cross sections for electron emission (DDCS) by heavy ion impact. The readily calculable form for numerical evaluation of the DDCS is given by eq 4.34 in ICRU.[24] The calculated DDCSs show a fairly good agreement with the experimental angular distributions for the ejected electrons with various energies for high-energy projectiles. However, the reproducibility for low-energy projectiles is unsatisfactory. Because the theoretical and model fitting do not provide a satisfactory solution, it is then realistic to use random sampling of angular distributions of ejected electrons from the experimental and interpolated data.

Available experimental angular distributions of electrons ejected from water by helium ion impact are limited. Toburen

TABLE 2: Experimental Data Used for Sampling Angular Distributions of Secondary Electrons

ion energy range[a]		He^{2+}				He^{+}			
lower	upper	reference	beam type	beam energy[a]	no. of data sets[b]	reference	beam type	beam energy[a]	no. of data sets[b]
1	50	41	H^{+}	15	8	41	H^{+}	15	8
50	150	41	H^{+}	100	4	36	He^{+}	75	5
150	250	36	He^{2+}	200	6	36	He^{+}	200	4
250	400	36	He^{2+}	300	6	36	He^{+}	300	4
400	700	36	He^{2+}	500	5	36	He^{+}	500	5
700	1250	42	H^{+}	1000	6	42	H^{+}	1000	6
1250	2000	42	H^{+}	1500	6	42	H^{+}	1500	6

[a] keV u^{-1} units. [b] In the references, angular distributions for various ϵ ejected by a projectile impact of a beam energy are graphically given. One data set means a set of data $d^2\sigma(\epsilon,\theta)/d\epsilon\, d\Omega$ as a function of θ for one ϵ. The number of data sets is equal to that of ϵ.

TABLE 3: Statistics of Interactions for 100 keV Alpha-Particles

full slowing down tracks
alpha energy = 100 keV
no. of tracks = 100
ave range = 1246.63 nm

	no. of interactions by a primary ion		
	He^{2+}	He^{+}	He^{0}
elastic	382.9	1261.6	6343.7
ionization	6.1	434.5	2095.2
excitation	4.4	196.5	701.9
two-electron capture	2.0		
electron capture	21.9	426.4	
electron loss		11.4	416.2
two-electron loss			11.8

no. of interactions by secondary electrons (per primary ion)					
ion(12.6)	ion(14.8)	ion(18.5)	ion(32.4)	ion(539.7)	excitation
206.7	139.9	48.9	2.3	0.0	4310.4

no. of interactions (including elastic and secondary electrons)	17024.8
no. of secondary electrons/primary ion	2677.3
no. of elastic interactions by a primary ion	7988.2
no. of interactions by a primary ion (except elastic)	4328.4
no. of interactions by secondary electron/primary ion	4708.2
no. of electron interactions/secondary electron	1.76
no. of $e-H_2O^{+}$ pairs by a primary ion	2759.1
no. of $e-H_2O^{+}$ pairs by secondary electron	320.2
no. of $e-H_2O^{+}$ pairs (primary+secondary electron)	3079.3
W-value	32.5 eV

et al.[36] provides a graphical presentation of electron angular distributions in the range 0.3−2 MeV He^{+} and He^{2+}. To cover the broad ion energy range, available proton data were used assuming that differences of angular distributions between different ions are not very large. Evidence for this assumption is seen in the experiments of Toburen et al.[36,41,42] The proton data by Bolorizadeh and Rudd[41] (15 and 100 keV) and by Toburen and Wilson[42] (1 and 1.5 MeV) were used. Table 2 summarizes experimental data used for sampling angular distributions of secondary electrons. The impact energy of ions is distributed among one of seven bins to which the experimental "beam energy" belongs. The "number of data sets" relates to electron energies for which angular distributions were given in the literature. Interpolation was done for the intermediate energies of electrons. The angular distribution of ejected electrons is sampled by a storage and look-up method. Figure 7 presents a comparison of DDCSs for various electron energies between randomly sampled and experiments at $T = 500$ keVu^{-1} in which ϵ is the electron energy. Sampled values obtained from sampling 2×10^5 times were normalized for overall fitting to the experimental values. Considerable differences between He^{2+} (solid lines and ○) and He^{+} (dashed lines and ×) are seen for low-energy electrons. Again, we assumed the angular distributions of electrons ejected from the target molecule by He^{0} impact to be equal to that for He^{+}.

3.3. Excitation. Impact excitation data of all helium ions on water molecules are not available. Therefore, we tentatively use the model of Miller and Green[26] which gives excitation cross sections and mean excitation energy loss by proton impact on water. They assumed an analytical function for each excited level of the form

$$\sigma_e = \frac{\sigma_0 (Za)^{\Omega} (T - W)^{\nu}}{J^{\Omega+\nu} + T^{\Omega+\nu}} \tag{7}$$

where $\sigma_0 = 10^{-16}$ cm^2; $Z = 10$; and the parameters W, a, J, Ω, and ν for 28 excitation states are given in Table 3 of the literature.[26] Miller and Green[26] noted that their excitation cross sections were only a rough estimate proposed in the absence of detailed theoretical or experimental data. They further noted that the position and height of the maximum in the cross section could easily be in error by a factor of 2 and that the nature of the low-energy falloff was speculative.

Figure 8 shows the calculated total excitation cross section as a function of helium energy. We have assumed cross sections for protons can be applied to the impact excitation cross sections

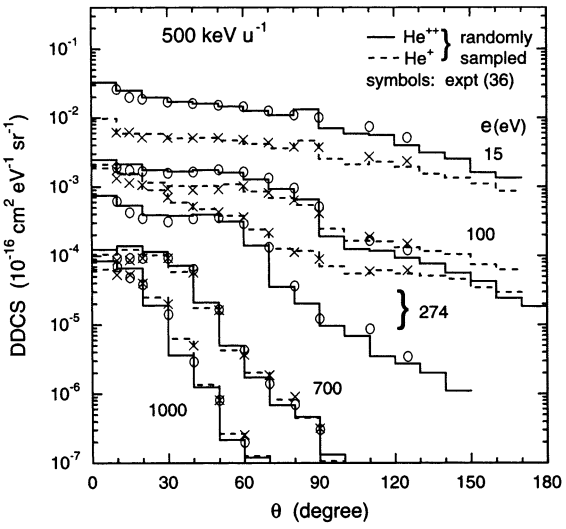

Figure 7. Comparison of angular distributions of secondary electrons for various electron energy ϵ (eV) ejected by 500 keVu^{-1} helium ion impact. The symbols are the experimental data of Toburen et al.[36] The lines are the results obtained from sampling 2×10^5 times from these data using the direct sampling method.

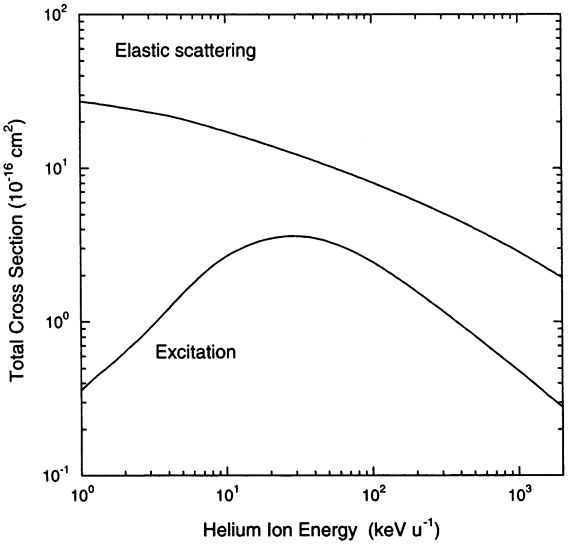

Figure 8. Total cross sections for elastic scattering and excitation due to alpha-particle impact on water vapor. Elastic scattering cross sections were evaluated by the classical-mechanics trajectory calculations. The excitation cross sections were calculated assuming model of Miller−Green for protons.[26] These cross sections were commonly used for all helium ions.

for all three hellium ions (He^{2+}, He^{+}, and He^{0}). Although this assumption may seem to be too naive, the fractional energy deposition due to excitation is at most about 10% for the overall energy range. Therefore, a serious inconsistency does not occur. The mean excitation energy Q_e was calculated using the relationship $\Sigma W_j\sigma_{ej}/\Sigma\sigma_{ej}$, where W_j is the excitation threshold energy and σ_{ej} is the excitation cross section for the state j given by Miller and Green.[26] The values of Q_e increase slowly from about 12 eV at 1 keVu^{-1} to 14 eV for the highest particle energies.

3.4. Elastic Scattering. The interaction between the projectile and the target atom can be described in terms of a potential function[51]

$$V(r) = \frac{zZe^2}{r} F_s(r/r_s) \tag{8}$$

The first factor in eq 8 is the Coulomb potential for two bare nuclei with charge ze and Ze. The factor $F_s(r/r_s)$ takes into account the screening by atomic electrons. The extent of screening is characterised by the screening length r_s. A commonly used prescription for the screening length is given by

$$r_s = 0.88534a_0(z^{0.23} + Z^{0.23})^{-1} \tag{9}$$

where a_0 is the Bohr radius and 0.88534 is a numerical constant from the Thomas−Fermi model of the atom. A screening function $F_s(r/r_s)$ for alpha-particles is given by Ziegler et al.[45]

$$F_s(r/r_s) = 0.1818e^{-3.2r/r_s} + 0.5099e^{-0.942r/r_s} + 0.2802e^{-0.4029r/r_s} + 0.2817e^{-0.2016r/r_s} \tag{10}$$

For a particle scattered in a central potential $V(r)$, the deflection angle θ is obtained in a classical-mechanics trajectory calculation as a function of the impact parameter p[46]

$$\theta = \pi - 2\int_{r_{min}}^{\infty} \frac{p}{r^2\sqrt{1 - V(r)/T_{cm} - p^2/r^2}}\,dr \tag{11}$$

where r_{min} is the distance of the closest approach. The positive root of the following relationship gives this value in which

$$r^2 - 2zZr_e\frac{m_ec^2}{\beta Pc}rF_s(r/r_s) - p^2 = 0 \tag{12}$$

$$\beta = \sqrt{1 - \left(\frac{m_\alpha c^2}{T + m_\alpha c^2}\right)^2} \tag{13}$$

$$Pc = \sqrt{(T + m_\alpha c^2)^2 - (m_\alpha c^2)^2} \tag{14}$$

and $r_e = 2.81794 \times 10^{-13}$ cm, m_ec^2 = electron rest mass, $m_\alpha c^2$ = alpha-particle rest mass ,and P is the momentum of alpha-particle. T_{cm} is the particle energy in the center-of-mass system, given by

$$T_{cm} = \frac{T}{1 + m_\alpha/M_t} \tag{15}$$

where T is the energy in the laboratory system and m_α and M_t are the masses of alpha-particle and target molecules. Equation 11 was solved numerically using procedures given by Everhart et al.[47] and Wilson and Haggmark.[48] The deflection angle θ was thereby obtained as a function of the impact parameter p. The boundary of "large-angle calculations" and "small-angle calculations" described by Everhart et al. was set at $\theta = 0.1\pi$ where smooth transitions are obtained.

The differential elastic scattering cross sections are given by[49]

$$\frac{d\sigma_{el}}{d\Omega} = -\frac{p}{\sin\theta}\frac{dp}{d\theta} \tag{16}$$

where θ and $d\sigma_{el}/d\Omega$ are functions of the impact parameter and the particle energy. Equation 16 was solved by numerical differentiation of the curve of the impact parameter versus the deflection angle using a B-spline interpolation. The total cross section for the particle energy T is calculated by

$$\sigma_{el}(T) = 2\pi\int_{\theta_{cut}}^{\pi} \frac{d\sigma_{el}}{d\Omega}\sin\theta\,d\theta \tag{17}$$

in which θ_{cut} was set to avoid the divergence in the scattering probability at low scattering angles[50]

$$\theta_{cut} \approx \frac{1}{137} Z^{1/3} \frac{m_e c^2}{Pc} \tag{18}$$

The total elastic scattering cross sections of alpha-particles in water is shown in Figure 8. Scattering angle θ is randomly sampled by a table of storage and look-up method in the Monte Carlo track code. We approximated both total and differential elastic scattering cross sections for He^+ and He^0 to be equal to that for alpha-particles.

3.5. Stopping Cross Sections. *3.5.1. Electronic.* The reliability of cross sections appropriate to the macroscopic stopping of low-energy alpha-particles in water were examined. We also performed analytical calculations of electronic and nuclear stopping cross sections for low-energy alpha-particles. The electronic stopping cross section S_e for alpha-particles is defined by

$$\begin{aligned} S_e = {} & F_2[\sigma_{i,++}(\bar{\epsilon}_{++} + \bar{B}_{H_2O}) + \sigma_e Q_e + \sigma_{20} Q_{20} + \sigma_{21} Q_{21}] \\ & + F_1[\sigma_{i,+}(\bar{\epsilon}_{+} + \bar{B}_{H_2O}) + \sigma_e Q_e + \sigma_{10} Q_{10} + \sigma_{12} Q_{12}] \\ & + F_0[\sigma_{i,0}(\bar{\epsilon}_0 + \bar{B}_{H_2O}) + \sigma_e Q_e + \sigma_{01} Q_{01} + \sigma_{02} Q_{02}] \end{aligned} \tag{19}$$

in which F denotes equilibrium charge fractions and σ denotes total cross sections, $\bar{\epsilon}$ is the average energy of secondary electrons by ion impact, and $\bar{B}_{H_2O}$ is the average binding energy of water molecule (Figure 5). The average energy by neutral-helium impact $\bar{\epsilon}_0$ was assumed to be equal to $\bar{\epsilon}_+$. Mean energy transfer Q_{if} in charge exchanges were modeled as

$$\begin{gathered} Q_{20} = 2\bar{B}_{H_2O} + 2\frac{T}{\lambda} - 2\bar{B}_{He}, \quad Q_{21} = \bar{B}_{H_2O} + \frac{T}{\lambda} - \bar{B}_{He} \\ Q_{10} = \bar{B}_{H_2O} + \frac{T}{\lambda} - \bar{B}_{He}, \quad Q_{12} = \bar{B}_{He} \\ Q_{01} = \bar{B}_{He}, \quad Q_{02} = 2\bar{B}_{He} \end{gathered} \tag{20}$$

in which $\bar{B}_{He}$= 24.59 eV is the average binding energy of a helium atom. This energy transfer model is consistent with the energy deposition model (eqs 1 and 2).

Equilibrium charge fractions, F_2, F_1, and F_0 for He^{2+}, He^+, and He^0, respectively, are given by Allison[32] as follows:

$$\begin{gathered} F_2 = [(a-b)\sigma_{20} + g(a+\sigma_{21}) - f(b+\sigma_{21})]/D \\ F_1 = (b\sigma_{20} - g\sigma_{21})/D \\ F_0 = (f\sigma_{21} - a\sigma_{20})/D \end{gathered} \tag{21}$$

in which

$$\begin{gathered} \alpha = \sigma_{01} + \sigma_{02}, \quad \beta = \sigma_{10} + \sigma_{12} \\ a = -(\beta + \sigma_{21}), \quad b = \sigma_{01} - \sigma_{21}, \quad f = \sigma_{10} - \sigma_{20}, \\ g = -(\alpha + \sigma_{20}) \\ D = ag - bf \end{gathered} \tag{22}$$

All parameters can be evaluated using the six types of cross sections for charge exchange as shown in Figure 1.

3.5.2. Nuclear. The nuclear stopping cross section S_n for alpha-particles of energy T is given by

$$S_n = 2\pi \int_{\theta_{cut}}^{\pi} \frac{d\sigma_{el}}{d\Omega} W(\theta,T) \sin\theta \, d\theta \tag{23}$$

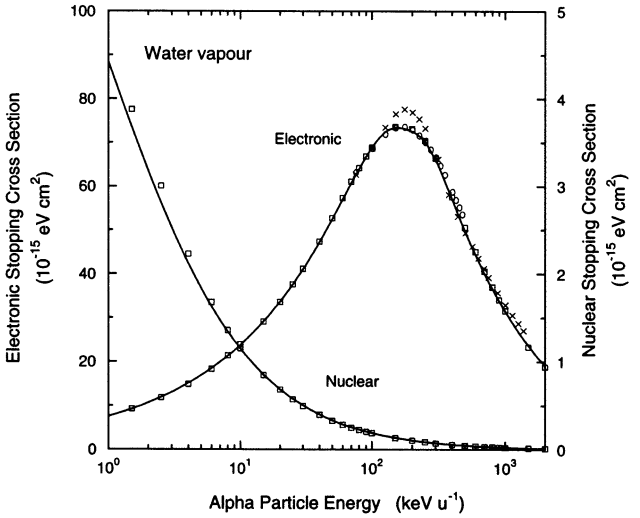

Figure 9. Comparison of the electronic and the nuclear stopping cross sections of water vapor as a function of the impact energy of the alpha-particles. (—) present calculations, (□) ICRU Report 49,[38] (○) Matteson et al.[51], (×) Thwaites.[52]

in which the energy transfer to the recoiling atom $W(\theta,T)$ is evaluated by

$$W(\theta,T) = 4T \frac{m_\alpha M_t}{(m_\alpha + M_t)^2} \sin^2 \frac{\theta}{2} \tag{24}$$

Figure 9 shows the calculated electronic (left ordinate) and nuclear (right ordinate) stopping cross sections in 10^{-15} eV cm^2 units of water vapor in comparison with the published data.[38,51,52] Both stopping cross sections agreed well with the ICRU tabulations.[38]

4. Results

4.1. Range and *W*-Values. The code *leahist* (*l*ow *e*nergy *a*lpha-particles *his*tory *t*racks) simulates the full slowing down of alpha-particles, following the primary ion down to a cutoff energy of 1 keV, at which point the residual energy is deposited at a random short distance. All electron interactions were followed down to 1 eV. To confirm the reliability of the simulated tracks and the code, calculations of the range and the *W*-values of alpha-particles were performed. The calculated alpha-particle ranges in water vapor (density = 1 g cm^{-3}) shown in Figure 10, agrees with the CSDA (continuous-slowing-down-approximation) ranges of ICRU[51] within a few percent deviation for the starting energy of alpha-particles between 1 keV (0.25 keVu^{-1}) and 8 MeV (2 MeVu^{-1}). This result is to be expected because the total stopping powers are in good agreement with the ICRU data as shown in Figure 9.

The *W*-value is defined as the mean energy expended in a gas per ion-pair formed. *W* is the quotient of *T* by *N*, where *N* is the mean number of ion-pairs formed when the initial kinetic energy *T* of a charged particle is completely dissipated in the gas. The value of *N* was obtained by scoring the ion-pairs due to ionization and charge exchange cycle, by taking into account the ionization events by the energetic secondary electrons ($\epsilon >$ 12.62 eV). Experimentally, *W*-values are derived by measuring the liberated electrons not H_2O^+. Detection of electrons with energies as low as a few eV is very difficult. Supposing such a limitation of measurement, it was assumed the e−H_2O^+ pair accompanied a very low-energy electron did not form a pair. We have introduced a lower limit of 0.75 eV for the formation of an electron−ion pair. The number of electron−ion pairs

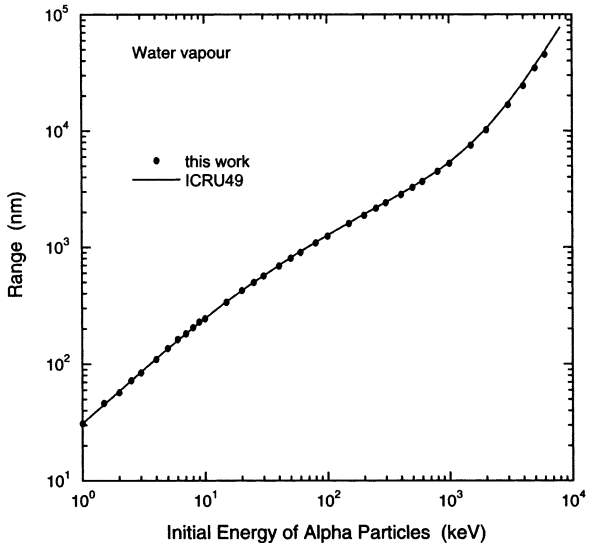

Figure 10. Calculated alpha-particle ranges as a function of energy and comparison with the ICRU data.[38]

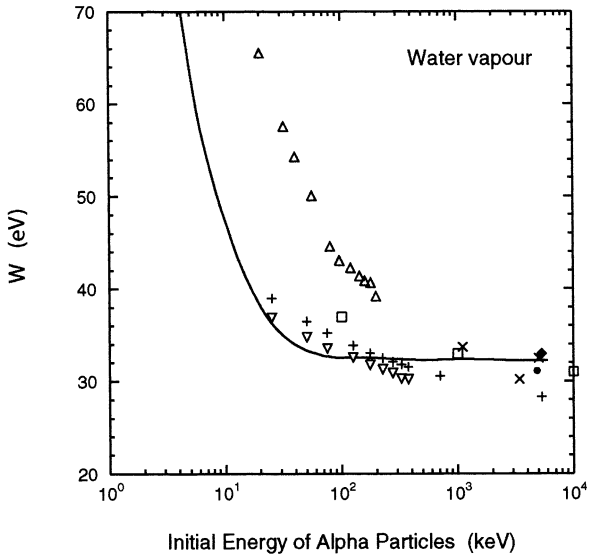

Figure 11. (—) Calculated *W*-values for alpha-particles in water vapor as a function of the initial energy in comparison with various experimental data: ● (ref 53), □ (ref 54), × (ref 55), △ (ref 56), ▽ (ref 57), ♦ (ref 58), + (ref 59). The present *W-value* of 32 eV at the high energy limit was close to the experimentally determined asymptotic limit, 31 eV recommended by the ICRU Report 31.[54]

produced by the secondary electrons exceeds that of pairs produced by alpha track itself at the initial energy around 2 MeV, where the number of electron induced pairs amounts to 36,000 per alpha-particle. The ratio of annihilated pairs to total generated pairs was 8% at 2 MeV. Figure 11 shows the calculated *W-values* in comparison with various published data.[53−59] We do not observe a flat minimum in energy dependence of *W*-values for alpha-particles as appeared for protons in CO_2 and N_2.[60] A *W*-value of 32 eV at the high energy limit was almost the same as the recommended value of 31 eV by ICRU.[54] The present *W*-values agree with published experimental data within a few percent of accuracy. It is difficult to conclude the validity of the code only from comparison of *W*-values, because experimental *W*-values obtained by several groups show large discrepancies for low-energy alpha-particles below 1 MeV.

4.2. Model Calculations. Figure 12 shows a gallery of two-dimensional representations of 1 MeV and 100 and 10 keV alpha tracks. These tracks include all seven types of interactions (elastic, ionizations, excitations, one- and two-electron capture, one- and two-electron loss) as listed in Table 1. An explicit number of interactions for 100 tracks of 100 keV alpha track is shown in Table 3. Data have been presented in terms of the number of interactions by the primary ion (alpha-particle) and by secondary electrons per primary alpha-particle. On each track are shown the interactions of primary particles and secondary electrons. Parts A and B show short segments of a 1 MeV tracks of proton and alpha-particle, clearly indicating the differences between the track properties and clustering of events for alpha and proton tracks of the same initial energies.

4.2.1. Radial Dose Distribution. Radial dose distribution, which is the energy absorbed locally at a certain radial distance from the path of a primary particle, has been used to check the reliability of track structure calculations. Figure 13 compares various data of the radial dose profiles around the path of 1 MeV (left part) and 3 MeV (right part) alpha-particles tracks. In this case, the energy depositions along the alpha track itself, i.e., "ion-potential", "excitation", "electron capture", and "elastic", are excluded in the dose calculations. Energies deposited only due to secondary electrons were accumulated within a coaxial shell with a radial interval of 0.5 nm along the alpha track from the origin to 210 and 900 nm for 1 and 3 MeV, respectively. The total energies deposited in these intervals of the alpha-particle range are 50 and 120 keV for 1 and 3 MeV, respectively. The secondary electrons consist of energetic electrons ejected by both ionization and electron loss processes. The contribution from the secondary electrons to the total absorbed dose is nearly 70% for energies greater than 1 MeV. This value is slightly larger for protons (67%)[23,42] in the energy region higher than 300 keV. The present calculations are compared with experimental data of Wingate and Baum[61] and two sets of calculated data of Butts and Katz[62] and of Wilson and Paretzke.[63] The measurements by Wingate and Baum were carried out for alpha-particles in tissue equivalent gas.

4.2.2. Restricted Stopping Powers. The energy restricted stopping power L_Δ is defined as that part of the total energy loss dE/dl which is associated with excitation-ionization energy transfers up to a cutoff value Δ.[64] Radius restricted stopping power, L_r, is defined as that part of the total energy loss dE/dl which is deposited within a cylinder of radius r and length dl, centered along the particle track. These are useful quantities for checking the reliability of track structure calculations. Whereas L_Δ can readily be calculated from basic differential cross sections by simple integration, it cannot be measured directly, radius restricted stopping power L_r can be measured directly but not readily calculated since complete track structure calculations are needed. The calculated ratios of L_Δ to L_∞ for the alpha-particles are almost the same as those for protons.[23]

Figure 14 shows the calculated ratio of L_r to L_∞ for the alpha-particle energies of 1, 2 and 3 MeV as a function of radial distance from the alpha-particle path. The track length, dl, was set at 210, 680, and 900 nm from the origin for $T = 1$, 2, and 3 MeV, respectively, in which the energy deposited amounts to $\sim$ 5% of the primary energy of alpha-particles. A large fraction of the energy lost by fast ions stays within the first nanometer around the path, but with increasing ion energy a large fraction can be transported by energetic electrons to large distances from that path. The present calculations for 2 and 3 MeV alpha-particles are in agreement with the experimental data of Wingate and Baum.[61] However, significant differences between the calculations and the experiments are found for 1

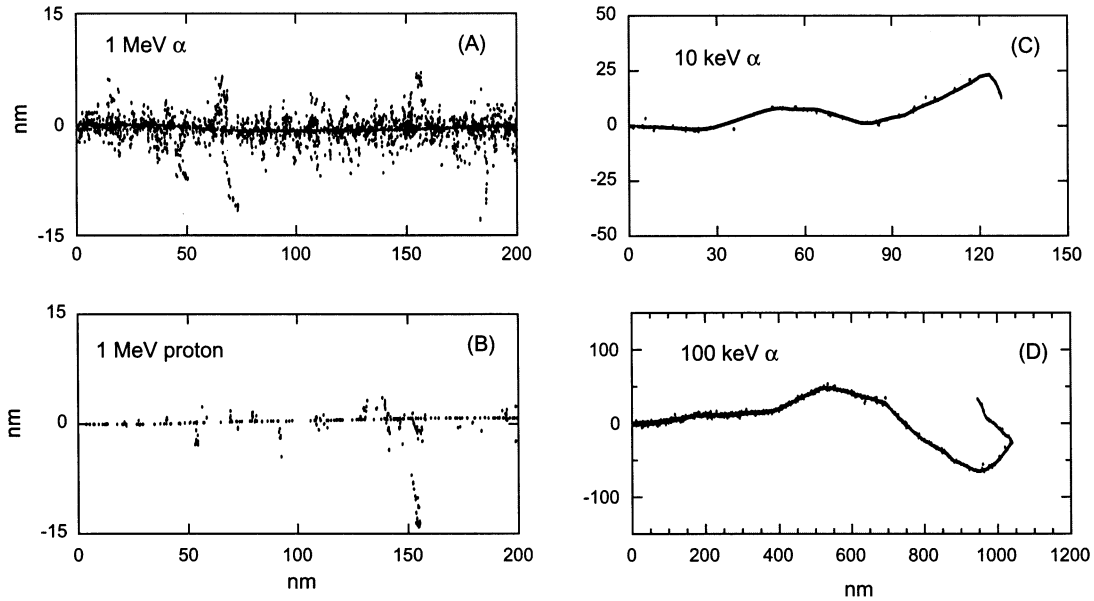

Figure 12. Two-dimensional examples of 1 MeV and 100 and 10 keV alpha and proton tracks (including elastic interactions) in water. Only the primary ion and the secondary electron interactions are shown. A complete list of the interactions is given in the Table 1.

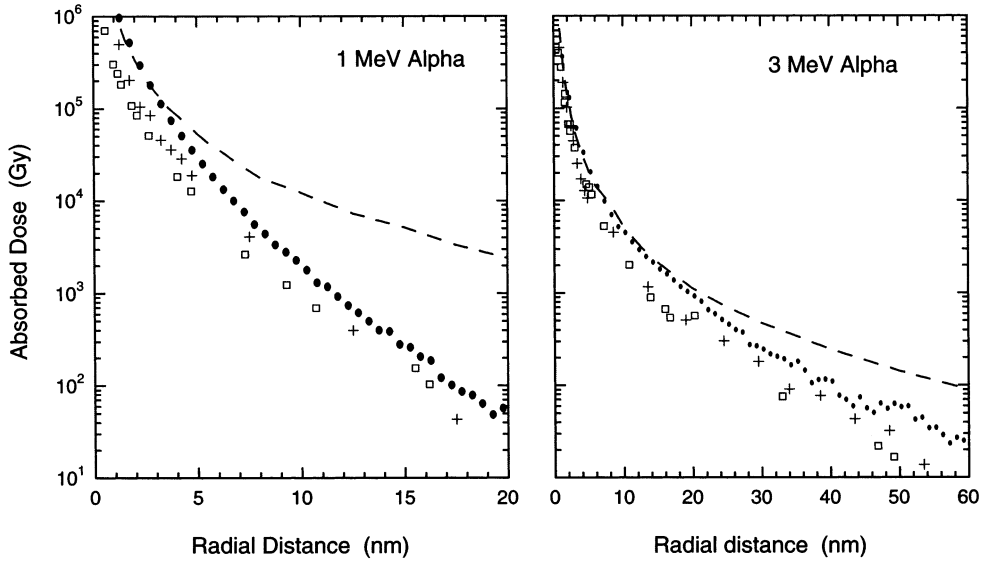

Figure 13. (●, this work) Calculated radial dose profiles around the alpha-particle path with energies (left part) 1 MeV and (right part) 3 MeV (compared to an experiment (□, ref 61), and the calculated data (− − −, ref 62 and +, ref 63). The experimental data of Wingate and Baum[61] were obtained for alpha-particles in tissue equivalent gas.

MeV alpha-particles. It is difficult to identify reasons for such discrepancies because of scarcity of cross sections for low-energy ions.

5. Discussion

The aim of this work was to simulate the full slowing down of alpha-particle tracks, molecular interaction by interaction, to be used for biophysical modeling in radiation physics, chemistry and biology. In these calculations we have made a number of assumptions which enabled us, for the first time, to simulate the full-slowing-down of alpha-particle tracks. Our analysis follows the established theoretical description of track structure theory and use of the existing knowledge, both experimental and theoretical, in an efficient way to achieve the objectives of the work. The assumptions adopted in the work arise from the fact that there are very few and insufficient cross section measurements available for low-energy ions and none below 1 keV. In the following subsections we discuss, elucidate some of the important points and assess the potential errors arising from such assumptions.

5.1. Cross Sections. As was stated earlier, there are insufficient experimental cross section data at low-energy ions. In this work we have extended the region of applicability of cross sections to lower energy regions. The first question we pose is to what extend extrapolation affects derivation of cross sections at low energies? There are uncertainties associated with extrapolation of He^{2+} cross sections to lower energies. However, the effect on the derivation of the He^0 cross sections from stopping power is negligible. Contribution of He^{2+} to the stopping power at the lower energies is very small because its equilibrium charge fraction is less than 1% below 20 $keVu^{-1}$. Therefore, calculations of the He^0 cross sections is not affected by extrapolation of the He^{2+} cross sections. The charge fraction of He^0 amounts to about 98% at 1 $keVu^{-1}$. The major

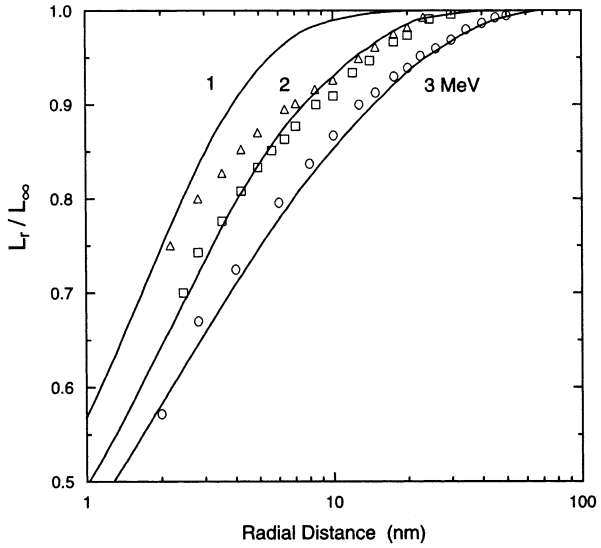

Figure 14. (—, this work) Calculated ratio of radius restricted stopping power L_r to unrestricted stopping power L_∞ for alpha-particle energies 1, 2, and 3 MeV as a function of the radial distance from the alpha-particle path in water. The experimental data (△, □, ○) of Wingate and Baum[61] were obtained for alpha-particles in tissue equivalent gas.

component (>90%) in the stopping power comes from He^0 ionization for energies less than 10 $keVu^{-1}$. All cross sections have uncertainties of about 10−20%.

A major assumption in this work is the use and the scaling of proton excitation cross sections. The second question is what are the potential uncertainties in assuming the excitation cross sections for He ions and neutrals to be the same as those for protons? The excitation component in the total electronic stopping power was ∼5% at 1 $keVu^{-1}$ and ∼13% at 20 $keVu^{-1}$. We have assumed the total excitation cross sections for He ions and neutrals are the same as those for protons. The potential error arising from this assumption needs to be assessed. Miller and Green have noted that the uncertainties associated with the total excitation cross sections is about a factor two.[26] To address this question, we recalculated the stopping powers by assuming twice the present cross sections for all ions (data not shown). Influence of these cross sections on the stopping power is at most about a 10% increase below the Bragg peak. The uncertainties in the excitation cross sections are estimated to be as much as 10% for the alpha tracks.

In the calculations of cross sections we have used the same equation for elastic scattering for He^+ and He^0 as He^{2+}. This assumption is supported by such experimental data that the magnitude of the cross sections for the bare and the neutral hydrogen with energies ∼10 keV is nearly the same.[25] Experimental data by Toburen supports this argument. There is no problem at high energies where bare helium ion is the dominant contributor to the total cross section.

In the absence and availability of cross sections, how did we obtain ionization cross sections for example for He^+ impact? Generally, ionization cross sections are determined by the measurements of secondary electron emissions with energies greater than a few eV. Therefore, the present data does not mean target ionization. Ionization cross sections for He^+ impact were obtained by subtracting the component of the secondary electrons produced by electron loss from the total electron emission. We have fitted the experimental ionization cross sections by using polynomial functions as was done for charge transfer. The slope of the log function for higher energy region was determined to reproduce the ICRU stopping powers, where He^{2+} impact ionization is the main contributor. In addition, use of the scaling law at these energies gives a justification for determining the slope. Figure 3 illustrates the applicability of Z^2 scaling between He^{2+} and H^+. Also, the extrapolation agrees with the theory for energies where charge-transfer processes are negligible. While, the slope at the lower energy region (<10 $keVu^{-1}$) may include ambiguities for He^{2+}, from the viewpoint of the stopping powers, the contribution of He^{2+} is negligible as the stopping powers below 30 $keVu^{-1}$ are dominated mainly by the He^0 component. Taking into account the reliability of the He^+ cross sections, the ionization cross sections were adjusted for the He^0 from the stopping power data. In the region below 30 $keVu^{-1}$, the stopping cross section for the He^{2+} is negligible and that for the He^0 is the main contributor. Reproducibility of stopping power data is the minimum criteria to judge the reliability of the cross sections. Data shown in Figure 8 justifies the reliability of cross sections, with 10−20% uncertainties, presented in this work.

Finally, we comment on the simultaneous electron loss plus target and projectile ionization. In a previous publication[21] we discussed this question. Bob DuBois has published data for He^+ in He gas[65] and found that He target ionization occurred in about 50% of the electron loss collisions from 175 to 500 $keVu^{-1}$ and then decreased to about 15% at 37.5$MeVu^{-1}$. There are no other data available for targets other than helium. Another set of data on single and double ionization of helium by hydrogen-atom impact is given by DuBois and Kover.[66] The fraction of target ionization occurring simultaneously ranged from about 4% at 25 keV to about 30% at 100 keV, increasing to about 70% at 800 keV. In the low-energy region, where H° is a reasonable fraction of the equilibrium charge, multiple ionization is approximately less than 25%. This is based on helium targets and might be higher for water where the binding energy is less than that for the helium target.

5.2. Secondary Electrons. The model of Rudd is correct for the lower energy region but underestimates the average energy of secondary electrons for higher energies. We have tested this using the simple Rutherford model:[24]

$$\frac{d\sigma_R(\epsilon)}{d\epsilon} = \frac{4\pi a_0^{\,2} Z_1^{\,2} R^2}{(T/\lambda)(\epsilon + B)^2} \tag{25}$$

where a_0 is the Bohr radius, Z_1 the nuclear charge of the incident particle, R is the Rydberg energy, and T/λ the kinetic energy of an electron with the same speed as that of the incident particle having the energy T. The Rutherford formula produces a better average energy for high energy He^{2+}. However, the spectral shape does not agree with the experimental data. The electron spectra calculated by the Rudd model are in good agreement with the experimental data as shown in Figure 6. This is the reason that we have based our calculations on the model of Rudd.

Equation 6 was derived from the experimental ratio of SDCSs of water vapor by He^+ to those for He^{2+} as a function of the ejected electron energy.[36] The ratios for various projectile energies, 0.2 to 0.5 $MeVu^{-1}$, show a linear relationship versus ϵ within around 10% deviation. We have approximated them by a linear function $g(\epsilon)$ and used it for all projectile energies.

The boundary energy of secondary electrons was set to1 eV. If the energy of a secondary electron is higher than 1 eV, that electron is regarded as an independent electron and its energy, position and direction are stored in the table for the secondary electrons. Otherwise, that electron energy (<1 eV) is added to the binding energy of the electron such that $\Delta E = B_i + \epsilon$.

Do uncertainties in angular distribution of low-energy electrons cause a serious effect on the particle track simulation? The similarity of H^+ and He^{2+} induced electron angular distributions for 300 $keVu^{-1}$ and 500 $keVu^{-1}$ is shown in Figure 4 of Toburen et al.[36] A small discrepancy is seen between H^+ and He^+ for several electron energies. We assumed all H^+ data can also be applied to He^{2+} including the low-energy region. For 500 $keVu^{-1}$ He^+, small differences are seen only for the backward emission at $\epsilon = 274$ eV; therefore, H^+ data may approximately be used for higher He^+ energies. As experimental data of He^+ is unavailable in the range below 50 $keVu^{-1}$, the H^+ data have been used in this energy region. Similarly, He^0 data over the whole energy range is also lacking. We assumed the angular distributions of electrons produced by the He^0 impact to be similar to that for the He^+. The uncertainties of angular distributions of low-energy electrons do not cause serious effect on the track structure because of their short ranges.

In this work, we approximated that the stripped electrons are emitted in the same direction as the projectile. We justify the approximation in the following manner. Experimental angular distribution of the stripped electrons for 150 keV $H^\circ + H_2O$ are given by Bolorizadeh and Rudd.[35] Figure 3 of their paper shows the relative size of the ELC (electron loss to the continuum). The intensity ratio between 0° and 150° is about 100. In addition, the intensity at 15° decreases about a tenth of that at 0 degree. Therefore, we approximated that the stripped electron is emitted with the same direction as the projectile. The effect on the track structure is negligible because the number of stripped electrons are very small in comparison with those generated by ionization as shown in Table 3.

5.3. Mean Energy Transfer. In general, stopping power, being a macroscopic quantity, is usually calculated using various averaged values such as potential energy, secondary electron energy and excitation energy. These energies are represented by the mean excitation energy in the standard formula. It is rather difficult, if not impossible, to discuss energy conservation event by event. Equation 20 conserves energy in the sense of an average quantity. We assumed the average potential energy for the doubly ionized water molecule as $\bar{B}_{H_2O}{}^{++} = 2\bar{B}_{H_2O}{}^{+}$.

In the model of mean energy transfer for charge exchanges, we used the term "average binding energy" in the sense of the average energy required or released when the charge state of the helium atom changes. The average binding energy for one- or two-electron transfer was expressed as $\bar{B}_{He}$ or $2\bar{B}_{He}$ for all ions. This assumption is reasonable for the initially neutral helium atom (He^0) because the relevant energy for formation of singly (He^+) or doubly (He^{2+}) ionized states becomes $\bar{B}_{He}$ or $2\bar{B}_{He}$, respectively. On this topic a number of questions could be asked: how good is the choice of the binding energies for He^+ and He^{2+}? Is the energy required for the formation of He^{2+} by an electron loss from He^+ the same as that for formation of He^+ from He^0? Is the energy released by one- or two-electron capture the same as the energy required for one- or two-electron loss for the electron capture occurring for He^+ and He^{2+}? To address these problems adequately, we need accurate data for He^+ and He^{2+}. However, even the use of accurate values for binding energies may not produce appreciably different results, because we are using binding energies averaged over all orbits.

6. Conclusions

In this paper we described in detail, for the first time, the development of a new generation of Monte Carlo track structure codes for the full-slowing-down of alpha-particles in the energy range 1 keV to 8 MeV. We described the model for the calculation of cross sections at lower energies. The cross sections and the energy transfer data were individually evaluated for the principal interactions induced by the bare and dressed ions, He^{2+}, He^+, and He^0, in water. The code *leahist* provides coordinates of all molecular interactions, amount of energy deposited along the track and the type of interaction at each event, as listed in Table 1. Despite adopting a number of assumptions in compiling the basic data necessary for simulation of track structure, especially for the excitation and the neutral-helium interactions, the macroscopic results, such as stopping powers, ranges, and W-values, provide good agreements with the experimental data and other calculations. Our data on stopping cross sections are in agreement with the published ICRU data. In summary, we have presented cross sections, single and doubly differential, and stopping powers needed for simulation of the full slowing down track of low-energy alpha-particles. We have presented model calculations using macroscopic radiation quantities, such as stopping power, W-values, and radial distribution of interactions, to provide verification of the code. Finally, we presented a comprehensive assessment of the potential errors and uncertainties associated with the principle components of the model. This new development enables us to work on the biophysical aspects of ionising radiation of environmental interests such as radon and mechanistic interpretation of experiments with neutrons. Further, developments such as this provides a tool to investigate the chemistry of low-energy ions in the chemical and biological environments.

Acknowledgment. We are most indebted to Larry Toburen, Walt Wilson and Alan Edwards for their expert advice and encouragement with this work. The work was partially supported by Grant-in-Aid for Scientific Research Contract (C) 12680503 from the Ministry of Education, Science, Sports and Culture of Japan, and the Commission of the European Communities Contract FIGH-CT-1999-00005.

References and Notes

(1) Pimblott, S. M.; LaVerne, J. A.; Mozumder, A.; Green, N. J. B. *J. Phys. Chem.* **1990**, *94*, 488.
(2) Pimblott, S. M.; Mozumder, A. *J. Phys. Chem.* **1991**, *95*, 7291.
(3) Pimblott, S. M.; LaVerne, J. A.; Mozumder, A. *J. Phys. Chem.* **1996**, *100*, 8595.
(4) Pimblott, S. M.; LaVerne, J. A. *J. Phys. Chem.* **1991**, *95*, 3907.
(5) Nikjoo, H.; Uehara, S.; Wilson, W. E.; Hoshi, M.; Goodhead, D. T. *Int. J. Radiat. Biol.* **1998**, *73*, 355.
(6) Nikjoo, H.; O'Neill, P.; Terrissol, M.; Goodhead, D. T. *Radiat. Environ. Biophys.* **1999**, *38*, 31.
(7) Paretzke, H. G. *Kinetics of Nonhomogeneous Processes*; Freeman, G. R., Ed.; Wiley: New York, 1987; pp 89−170.
(8) Turner, J. E.; Magee, J. L.; Wright, H. A.; Chatterjee, A.; Hamm, R. N.; Ritchie, R. H. *Radiat. Res.* **1983**, *96*, 437.
(9) Terrissol, M.; Beaudre, A. *Radiat. Prot. Dosim.* **1990**, *31*, 171.
(10) Uehara, S.; Nikjoo, H.; Goodhead, D. T. *Phys. Med. Biol.* **1993**, *38*, 1841.
(11) Lappa, A. V.; Bigildeev, E. A.; Burmistrov, D. S.; Vasilyev, O. N. *Radiat. Environ. Biophys.* **1993**, *32*, 1.
(12) Hill, M. A.; Smith, F. A. *Radiat. Phys. Chem.* **1994**, *43*, 265.
(13) Wilson, W. E.; Paretzke, H. G. *Radiat. Res.* **1981**, *87*, 521.
(14) Wilson, W. E.; Metting, N. F.; Paretzke, H. G. *Radiat. Res.* **1988**, *115*, 389.
(15) Zaider, M.; Brenner, D. J.; Wilson, W. E. *Radiat. Res.* **1983**, *95*, 231.
(16) Chatterjee, A.; Holley, W. *Adv. Radiat. Biol.* **1993**, *17*, 181.
(17) Cobut, V.; Frongillo, Y.; Patau, J. P.; Goulet, T.; Fraser, M.-J.; Jay- Gerin, J.-P. *Radiat. Phys. Chem.* **1998**, *51*, 229.
(18) Wilson, W. E.; Nikjoo, H. *Radiat. Environ. Biophys.* **1999**, *38*, 97.
(19) Emfietzoglou, D.; Papamichael, G.; Moscovitch, M. *J. Phys.* **2000**, *D33*, 932.
(20) Nikjoo, H.; O'Neill, P.; Goodhead, D. T.; Terrissol, M. *Int. J. Radiat. Biol.* **1997**, *71*, 467.

(21) Uehara, S.; Toburen, L. H.; Wilson, W. E.; Goodhead, D. T.; Nikjoo, H. *Radiat. Phys. Chem.* **2000**, *59*, 1.
(22) Dingfelder, M.; Inokuti, M.; Paretzke, H. G. *Radiat. Phys. Chem.* **2000**, *59*, 255.
(23) Uehara, S.; Toburen, L. H.; Nikjoo, H. *Int. J. Radiat. Biol.* **2001**, *77*, 139.
(24) ICRU. Secondary Electron Spectra from Charged Particle Interactions. Report 55; International Commission of Radiation Units and Measurements: Bethesda, MD, 1996.
(25) Toburen, L. H. *Radiat. Environ. Biophys.* **1998**, *37*, 221.
(26) Miller, J. H.; Green, A. E. S. *Radiat. Res.* **1973**, *54*, 343.
(27) Uehara, S.; Nikjoo, H.; Goodhead, D. T. *Radiat. Res.* **1999**, *152*, 202.
(28) Rudd, M. E.; Goffe, T. V.; Itoh, A. *Phys. Rev.* **1985**, *A32*, 2128.
(29) Barnett, C. F.; Ray, J. A.; Ricci, E.; Wilker, M. I.; McDaniel, E. W.; Thomas, E. W.; Gilbody, H. B ORNL-5206. Oak Ridge National Laboratory: Oak Ridge, 1977; Vol. 1.
(30) Rudd, M. E.; Itoh, A.; Goffe, T. V. *Phys. Rev.* **1985**, *A32*, 2499.
(31) Sataka, M.; Yagishita, A.; Nakai, Y. *J. Phys.* **1990**, *B23*, 1225.
(32) Allison, S. K. *Rev. Mod. Phys.* **1958**, *30*, 1137.
(33) Rudd, M. E. *Phys. Rev.* **1988**, *A38*, 6129.
(34) Wilson, W. E.; Toburen, L. H. *Phys. Rev.* **1973**, *A7*, 1535.
(35) Bolorizadeh, M. A.; Rudd, M. E. *Phys. Rev.* **1986**, *A33*, 893.
(36) Toburen, L. H.; Wilson, W. E.; Popowich, R. J. *Radiat. Res.* **1980**, *82*, 27.
(37) Rudd, M. E.; Goffe, T. V.; DuBois, R. D.; Toburen, L. H. *Phys. Rev.* **1985**, *A31*, 492.
(38) ICRU. Stopping Powers and Ranges for Protons and Alpha Particles. Report 49; International Commission of Radiation Units and Measurements: Bethesda, MD, 1993.
(39) McDaniel, E. W.; Mitchell, J. B. A.; Rudd, M. E. *Atomic Collisions, Heavy Particle Projectiles*; Wiley: New York, 1993; Chapter 4.
(40) Barnett, C. F. *Atomic Data for Fusion*. ORNL-6086/V1; Oak Ridge National Laboratory: Oak Ridge, 1990; Vol. 1.
(41) Bolorizadeh, M. A.; Rudd, M. E. *Phys. Rev.* **1986**, *A33*, 888.
(42) Toburen, L. H.; Wilson, W. E. *J. Chem. Phys.* **1977**, *66*, 5202.
(43) Rudd, M. E.; Kim, Y.-K.; Madison, D. H.; Gay, T. J. *Rev. Mod. Phys.* **1992**, *64*, 441.
(44) Hansen, J. P.; Kocbach, L. *J. Phys.* **1989**, *B22*, L71.
(45) Ziegler, J. F.; Biersack, J. P.; Littmark, U. *The Stopping and Ranges of Ions in Matter*; Pergamon Press: Elmsford, New York, 1985; Vol. 1.
(46) Mott N. F.; Massey, H. S. W. *The Theory of Atomic Collisions*, 3rd ed.; Oxford University Press: London, UK, 1965.
(47) Everhart, E.; Stone, G.; Carbone, R. J. *Phys. Rev.* **1955**, *99*, 1287.
(48) Wilson, W. D.; Haggmark, L. G. *Phys. Rev.* **1977**, *B15*, 2458.
(49) Goldstein, H. *Classical Mechanics*; Addison-Wesley: Reading, MA, 1950.
(50) ICRU. Basic Aspects of High Energy Particle Interactions and Radiation Dosimetry. Report 28; International Commission of Radiation Units and Measurements: Washington, DC, 1978.
(51) Matteson, S.; Powers, D.; Chau, E. K. L. *Phys. Rev.* **1977**, *A15*, 856.
(52) Thwaites, D. I. *Phys. Med. Biol.* **1981**, *26*, 71.
(53) Rohrig, N.; Colvert, R. D. *Radiat. Res.* **1978**, *76*, 225.
(54) ICRU. Average Energy Required To Produce an Ion Pair. Report 31; International Commission of Radiation Units and Measurements: Washington, DC, 1979.
(55) Budd, T.; Marshall, M.; Kwok, C. S. *Radiat. Res.* **1981**, *88*, 228.
(56) Huber, R.; Combecher, D.; Burger, G. *Radiat. Res.* **1985**, *101*, 237.
(57) Posny, F.; Chary, J.; Nguyen, V. D. *Phys. Med. Biol.* **1987**, *32*, 509.
(58) Stonell, G. P.; Marshall, M.; Simmons, J. A. *Radiat. Res.* **1993**, *136*, 341.
(59) Bronic, I. K. *Radiat. Prot. Dosim.* **1997**, *70*, 33.
(60) Waibel, E.; Willems, G. *Phys. Med. Biol.* **1992**, *37*, 249.
(61) Wingate, C. L.; Baum, J. W. *Radiat. Res.* **1976**, *65*, 1.
(62) Butts, J. J.; Katz, R. *Radiat. Res.* **1967**, *30*, 855.
(63) Wilson, W. E.; Paretzke, H. G. *Proc. Fourth Symposium on Microdosimetry*, (J. Booz, H. G. Ebert, R. Eickel, and A. Waker, Eds.); Commission of the European Communities: Luxembourg, 1974; pp 113−122.
(64) ICRU. Linear Energy Transfer. Report 16; International Commission of Radiation Units and Measurements: Washington, DC, 1970.
(65) DuBois, R. D. *Phys. Rev.* **1989**, *A39*, 4440.
(66) DuBois, R. D.; Kover, A. *Phys. Rev.* **1989**, *A40*, 3605.